A 500-km Cascaded White Rabbit Link for High-Performance Frequency Dissemination

Namneet Kaur, Florian Frank, Jose Pinto, Philip Tuckey, Paul-Eric Pottie

A 500-km Cascaded White Rabbit Link for High-Performance Frequency Dissemination

Namneet Kaur, Florian Frank, Jose Pinto, Philip Tuckey, and Paul-Eric Pottie

***Abstract*— We perform experiments exploring the use of white rabbit precision time protocol (WR-PTP) for time and frequency dissemination over long-distance optical fiber links. We use unidirectional links, to ensure compatibility with active telecommunication networks, and White Rabbit equipment with modifications for improved performance. Using fiber spools, we realize a 500 km, four-span cascaded white rabbit link. We show short term fractional frequency stability of 2×10^{-12}, averaging down to 2×10^{-15} at one day of integration time, with no frequency shift within the statistical uncertainty. We demonstrate the impact of increasing the White Rabbit SoftPLL bandwidth and the PTP message rate. We show evidence of the effect of thermal fluctuations acting on the fiber, and finally discuss the limitations of the achieved performance. We show comparisons with experimental data acquired with commercial good quality global positioning system (GPS) receivers and show that the medium- and long- term stability and accuracy are more than one order of magnitude better with a WR-PTP link.**

***Index Terms*— Fiber optics, measurement and estimation uncertainty, synchronization (clock, frequency, network, phase, and time).**

I. Introduction

OVER the last fifteen years, optical fiber links have been intensively studied for frequency dissemination. They have demonstrated frequency transfer with fractional frequency stability and total uncertainties below 10^{-19} over several hundred km [1], [2]. This allows comparisons of optical signals with accuracy and stability down to the 10^{-20} level and the comparison of remote clocks with unprecedented uncertainty [3], [4], opening doors to new stringent tests of fundamental physics [5] and to the development of chronometric geodesy [6].

Manuscript received September 13, 2021; accepted December 3, 2021. Date of publication December 8, 2021; date of current version January 26, 2022. This work was supported in part by the LABoratoire d'EXcellence (LABEX) Cluster of Excellence Formation Innovation Recherche Services et Transfert Temps-Fréquence (FIRST-TF) within the Program d'Investissements d'Avenir under Grant ANR-10-LABX-48-01 and in part by BPIFrance under the Distribution légale, certifiée et traçable du temps (SCP Time) project. The experimental data shown for the global positioning system (GPS) receivers were acquired in the context of the European Union (EU) projects NEAT-FT and Optical Frequency Transfer-a European Network (OFTEN), funded by the European Metrological Research Program (EMRP) under Grant SIB-02 NEAT-FT and the European Metrology Programme for Innovation and Research (EMPIR) under Grant 15SIB-5 OFTEN. The EMRP and EMPIR are jointly funded by the EMRP/EMPIR participating countries within the European Association of National Metrology Institutes (EURAMET) and EU. *(Corresponding author: Paul-Eric Pottie.)*

The authors are with the LNE-SYRTE, Observatoire de Paris, Université PSL, CNRS, Sorbonne Université, 75014 Paris, France (e-mail: paul-eric.pottie@obspm.fr).

Digital Object Identifier 10.1109/TUFFC.2021.3134163

For the transfer of radio frequency (RF) references over optical fiber, a mature and high-performance approach exists, the ELSTAB technique [7], which uses active stabilization of the propagation delay for joint time and frequency transfer. Introduced ten years ago [8], [9], it allows time and frequency distribution from one server to a few remote sites [10]. Other methods for time and/or frequency transfer over optical fiber links are being developed for various applications by other research groups, with performances surpassing global navigation satellite system (GNSS) signal distribution [11], [12]. Such high-performance experiments require standard telecommunication links to be modified to support a fully bidirectional architecture, i.e., allowing the transmission of signals in both directions, at the same wavelength, within a single fiber. These methods are applicable to point-to-point or point-to-a-few network architectures.

Over the last decade there has also been an increasing demand for precise time and frequency distribution in areas such as particle physics, telecommunication, navigation, smart grid, high-frequency trading, and sensing [13]–[18]. To answer these demands, much experimental work is focusing on unidirectional architectures, i.e., using separate fibers for signal transmission in the two directions, exploiting wavelength division multiplexing (WDM). This allows a better signal-to-noise ratio but *a priori* a lower level of control of the asymmetry of the links [19]. Therefore, the uni-directional architecture offers a different tradeoff between performances and costs, in the optical and RF domains [20]–[23].

A very promising direction for time and frequency transfer over optical fiber links is the white rabbit precision time protocol (WR-PTP) [24], [25], for its scalability to massive multiple users, capacity to build redundant ring topologies, [26]–[28], and IEEE standardization under High-Accuracy profile of IEEE1588-2019 [29]. WR-PTP is suitable for coarse wavelength division multiplexing (CWDM) and dense wavelength division multiplexing (DWDM) fiber network, as demonstrated on long-haul links up to 1000 km [30], [31]. Much work has been done recently on improving WR performance and scalability, such as on lower jitter WR-PTP equipment, network supervision, precise calibration and better flexibility, and adaptability for industry [32]–[38].

With its promising timing capabilities and high performance, WR-PTP is being utilized for many scientific experiments ranging from time synchronization for particle detectors such as LHAASO, HiSCORE, KM3net, and CSNS, for radio astronomy and remote maser concepts (SKA, CTA, etc.), for trigger distribution systems (PMU), and for seismic

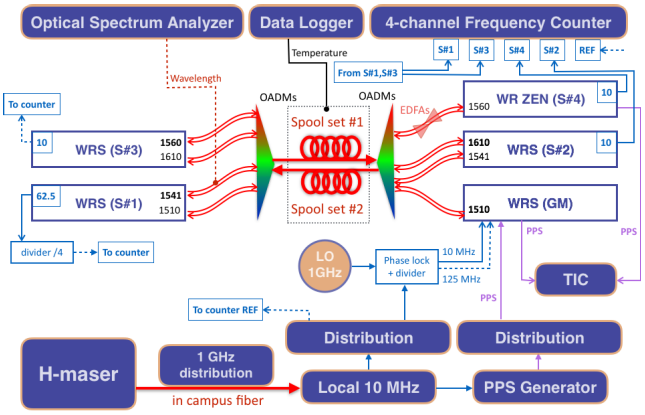

Fig. 1. Experimental setup for the 500-km cascaded WR link. The same pair of 125-km fiber spools are used at each stage of the cascaded link by employing OADMs. Each fiber spool consists of simplex single mode fiber. An optical spectrum analyzer and a data logger record the emitted wavelength and the temperature of the spools set simultaneously. All the frequencies are counted simultaneously, as well as the pulse per second (PPS) output at the last stage. LO: Local oscillator. TIC: Time interval counter. EDFA: Erbium-doped fiber amplifier. WRS: White-rabbit switch. OADM: Optical add-and-drop multiplexers. The WR devices are represented with numbers in blue box that refer to the clock output frequency in MHz and with numbers in black box that refers to the wavelength output of the SFP in nm (see text).

measurements at CERN [39], [40]. Many details can be found in [41]. Other scientific projects such as square kilometer array (SKA) [42] and Cherenkov telescope array (CTA) [43] are evaluating WR-PTP for their timing applications.

The work presented here focuses on using WR-PTP for multi-user and accurate frequency dissemination over long-haul links, typically of several hundred km. Since our objective is to serve multiple users, we focus on the uni-directional architecture which is compatible with active telecommunication networks. We demonstrate a 4-span, cascaded, 500-km White Rabbit link, operated in the laboratory using fiber spools. The cascaded approach was previously studied in the context of coherent optical links, one of the advantages being to improve the short-term stability [44]. In the context of WR-PTP, such cascaded links were studied in view of scalability [45]. In this work, we study the impact of software defined parameters on WR-PTP performance over long-haul fiber links and propose a cascaded approach in order to circumvent some limitations due to chromatic dispersion [19]. We provide a comparison with equivalent industrial-grade solutions based on GPS and discuss the results.

II. Experimental Setup

The experimental setup is illustrated in Fig. 1. The 10-MHz reference is generated from a home-made, in-campus RF optical link, disseminating the 1-GHz signal of an active H-Maser, and home-made low-noise frequency divider and distribution units, similar to the setup for generating UTC(OP) [46]. The short-term stability of the 10-MHz signal in our laboratory was evaluated to be at the level of 2×10^{-13} at one second of integration time in a 5-Hz bandwidth. A reference pulse per second (PPS) signal is generated from the 10-MHz signal using a PPS generator.[1] The PPS signal represents our local time scale. This reference PPS is input to an amplification and distribution unit.[2]

We use a set of ten 25-km fiber spools, connected together to build two 125-km uni-directional fiber links. We connect a multichannel coarse WDM filter at the entry and exit points of the fiber link, which allows adding or dropping up to five wavelengths of the telecommunication ITU grid. By utilizing different sets of transmission/reception (TX/RX) wavelengths for transport over the 125-km uni-directional links, we can concatenate WR-PTP links in series and build a cascaded 500-km long-haul link in the laboratory. We will refer to one transfer over a 125-km link as a span.

We use several generic small form factor pluggable (SFP) optical transceivers operating at different wavelengths of the ITU telecommunication *S*-band, *L*-band, and *C*-band. The central wavelengths of the emitters are 1510, 1541, 1560, and 1610 nm. 1541 and 1560 nm are combined using circulators and additional DWDM filters. Two uni-directional erbium-doped fiber amplifiers (EDFAs) with a gain of about 10 dB are used for the link at 1560 nm, which exhibited more losses than the others and less tolerance to the detected power.

All the WR-PTP equipment is manufactured by Seven Solutions. For our experiment, we use as Grandmaster a White Rabbit switch that we improved for high performance and low jitter by implementing a direct clock to the clock fan-out in the board [47]. The firmware was updated with the support of CERN. The Grandmaster (GM) White Rabbit switch receives the 10 MHz and PPS reference signals generated in the laboratory. The short-term stability of the improved GM with respect to the reference 10-MHz signal was measured to be as low as 5×10^{-13} at one second of integration time in a 50-Hz bandwidth. The performance and details of the implementation are described in [48]. We also measured the time deviation between one output of our PPS distribution unit and the PPS signal of the GM with a time interval counter[3] and obtained a time deviation of 5.5 ps at one second of integration time, which averaged down to below 1 ps after 30 s of integration time and remained below ps level up to several days of integration [49].

We use three White Rabbit switches as boundary clocks and a WR-ZEN as an end-user node [42], [50]. We labeled them as Slave #1 to #4, respectively. Using WDM, each equipment is assigned a specific emitting wavelength per 125-km span, allowing simultaneous cascaded transmission over the 2 km $\times$ 125 km uni-directional fiber span.

In this way, time and frequency are transferred from the Grand master to the Boundary switches and the end-user node in a hierarchical manner using a cascaded approach. The first Slave outputs a 62.5-MHz signal, which we divide by 4 before counting. The last three Slaves output a 10-MHz signal.

The 15.625-MHz output and the three 10-MHz outputs are recorded simultaneously by a dead-time free phase and frequency counter, operated in Λ mode with a one-second gate time.[4] All the Slaves output a PPS signal, but only the time

[1] SDI, PPS-2RM-B.

[2] TimeTech, 10276.

[3] Physipus STS201.

[4] K+K Messtechnik FXE

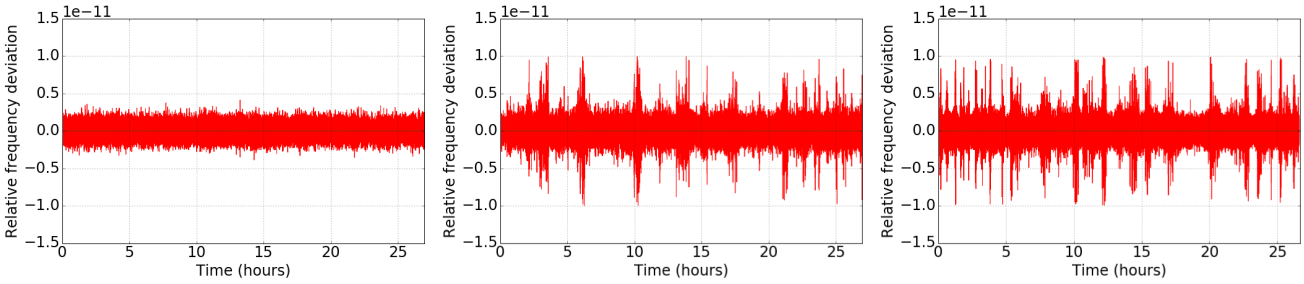

Fig. 2. Relative frequency deviation y for the first span of 125 km with (a) 14-Hz PTP rate and 70-Hz locking bandwidth (b) 1-Hz PTP rate and 70-Hz locking bandwidth, (c) 1-Hz PTP rate and 20-Hz locking bandwidth, over 1 00 000-s measurement time. Data with $|y| > 10^{-11}$ were considered as outliers and removed: none in case (a), 350 points in case (b), and 500 points in case (c). The green lines show the average value for each dataset.

TABLE I
PERFORMANCES OF A WHITE RABBIT LINK ARE COMPARED FOR THREE EXPERIMENTAL SITUATIONS. THE THREE CASES ARE LABELED FROM (A) TO (C), VARYING THE PTP MESSAGE EXCHANGE RATE AND THE BANDWIDTH OF THE SOFT PHASE-LOCKED LOOP

	(a)	(b)	(c)
f_{PTP} (Hz)	14	1	1
f_{BW} (Hz)	70	70	20

interval between the output PPS of the GM and the end-user ZEN are measured and recorded with a Physipus STS201, an event timer designed for the T2L2 experiment [51], [52].

The temperature of the experimental room is measured every 10 s with a 10-kOhms thermal sensor and recorded with a data logger.[5]

In addition, a 90/10 optical coupler is used to extract the wavelength of the 1541-nm optical emitter and it is recorded with a high-resolution optical spectrum analyzer.[6] All the data are recorded simultaneously.

In our setup, we applied two software modifications to improve the performance of the Slave switches, with binaries first prepared with the support of CERN, and that we flashed into the WRS [53]. First, we increased the bandwidth f_{BW} of the soft phase-locked loop (SoftPLL) to 70 Hz (default bandwidth = 20 Hz), as introduced in [54]. Second, we increased the PTP rate f_{PTP} of operation to 14 Hz (Default PTP rate = 1 Hz) [48]. To our knowledge, this is the first time that the effect of high PTP rate on frequency stability is reported.

III. EXPERIMENTAL RESULTS

A. Effect of Increased Locking Bandwidth and PTP Rate

We compare three choices for f_{BW} and f_{PTP}, summarized in Table I. Fig. 2 presents the relative frequency deviation, $y = df/f_0$, where df is the frequency fluctuation and f_0 is the carrier frequency of the clock output of the WR switch, for the first switch at 125 km. The measurement lasted for 12 consecutive days and produced 1 036 800 data points. The data were filtered within a range of $\pm 10^{-11}$.

Fig. 2 shows that with the higher locking bandwidth and higher PTP rate, we observe peak to peak deviations $< 5.0 \times 10^{-12}$. We observe degradation in performance with both decreasing PTP rate and SoftPLL bandwidth. The PTP rate was set as high as allowed by our WRS [48]. The SoftPLL bandwidth was set as high as possible, by varying the proportional and integrator gain of the loop and looking at the PSD of phase noise of the 10-MHz output signal and its fractional frequency stability. More details can be found in [49]. Optimization procedures of the SoftPLL were also reported in [55].

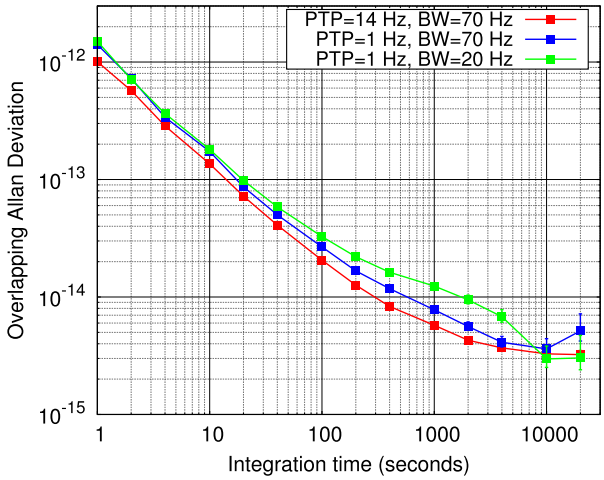

Fig. 3. OADEV for the clock output of the first span of 125 km. Red trace: $f_{PTP} = 14$ Hz, $f_{BW} = 70$ Hz. Blue trace: $f_{PTP} = 1$ Hz, $f_{BW} = 70$ Hz. Green trace: $f_{PTP} = 1$ Hz, $f_{BW} = 20$ Hz (default case).

Fig. 3 shows the overlapping Allan deviation (OADEV) [56] for the three cases. At one second of integration time, the stability is degraded by a factor of approximately 1.5 for cases (b) and (c). This is not limited by the filtering as we observe the same OADEV with a filtering range of $\pm 2.5 \times 10^{-11}$. We observe an excess of noise at 2000 s for the 1-Hz PTP rate and 20-Hz SoftPLL bandwidth case. At longer integration times, the OADEV are similar as another noise source starts to dominate.

From now onward, we use the PTP rate $f_{PTP} = 14$ Hz and the SoftPLL bandwidth $f_{BW} = 70$ Hz.

B. Effect of Temperature

We present the effect of temperature on the residual frequency deviations. From the frequency data acquired from the first Slave S#1, we integrate the relative frequency deviations y over the integration time to obtain the phase fluctuation as a function of time, denoted by Φ_{WR}, expressed as a time error

[5] Agilent 34972A.
[6] Yokogawa AQ6370C.

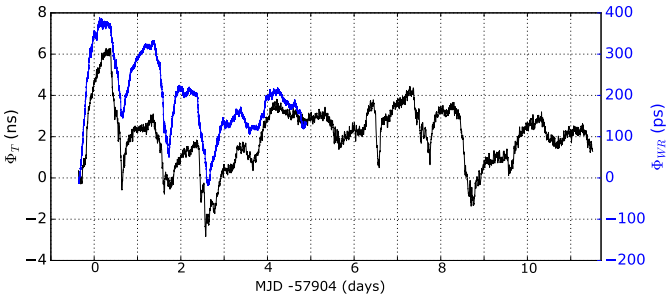

Fig. 4. Black trace, left axis: Propagation delay fluctuations Φ_T calculated from the temperature data, estimating the thermal noise contribution to the free running propagation noise of the 125-km fiber link, as a function of time expressed in modified Julian day (MJD). A linear drift of −3.85 fs/s is removed. Blue Trace, right axis: Time delay fluctuations Φ_{WR} at the Slave after the first 125-km span. Note that the vertical scales are, respectively, in ns and ps.

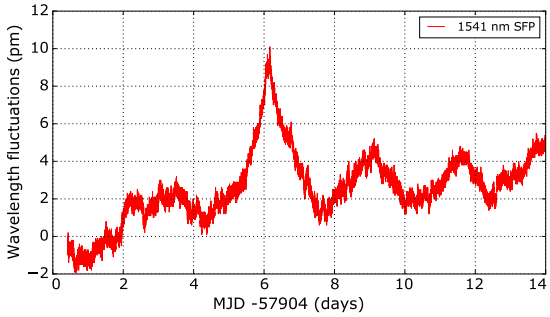

Fig. 5. Wavelength fluctuations of the 1541-nm SFP over 14 days of continuous measurement.

in units of s. In the following, we also refer to this quantity as the time delay fluctuation.

The time delay fluctuations are presented in Fig. 4 as the blue trace, for the WR switch used as the boundary clock for the first span, after 125 km. 29 outliers were removed from the dataset. The peak-to-peak fluctuations are about 400 ps over 12 days of measurement. We mention that similar behavior is observed at all stages of the cascaded link, with a scaling behavior described later on. At the last stage of the cascaded link, the time delay fluctuations reach 2.5 ns.

As the temperature fluctuations were acquired simultaneously over the same time period (see Section II) they can be compared directly with the delay fluctuations Φ_{WR}. In order to calculate the contribution of the temperature to the free running propagation noise of the fiber link, we calculate the propagation delay fluctuations that arise from the temperature fluctuations, by taking into account the length of our link, and the fiber temperature sensitivity factor of 37 fs/K/m [57], [58]. The temperature fluctuation is defined as $\Delta T_i = T_i - T_0$, where ΔT_i is the temperature fluctuation time series, T_i the temperature time series, and T_0 the first temperature measurement. The temperature fluctuation data are smoothed with a rolling time window of 100 points, i.e., in a time window of about 20 min. A linear drift of −3.85 fs/s is removed. We denote the resulting free running propagation delay fluctuations arising from temperature as Φ_T. As shown in Fig. 4, black trace, the peak-to-peak free running propagation delay fluctuations are about 10 ns over the same 12 days of measurement. The correlation coefficient between Φ_{WR} and Φ_T is $\simeq 90\%$.

C. Effect of Chromatic Dispersion

We studied the effect of the laser frequency instability combined with the chromatic dispersion of the fiber, at both short and long integration time. The linewidth of the SFP emitters was measured simultaneously with an Optical Spectrum Analyzer (see Section II). The spectral line was fit with a Gaussian profile. The full-width at half-maximum of the Gaussian profile is 0.024 nm (3 GHz) at 4 s of integration time, significantly limited by the resolution bandwidth of the measurement device. We found similar line widths for the other CWDM SFPs built with similar DFB lasers (but not recorded at the same time). For comparison, for a temperature-stabilized DFB laser such as integrated into the DWDM long-range SFPs, the linewidth at one second of integration time is expected to be in the range of 1 – 100 MHz.

The chromatic dispersion contribution at long term can also be estimated with our setup, as the wavelength of the emitter was measured over the same time period. We performed a measurement of the central wavelength every 60 s. We denote the wavelength fluctuations as $\delta\lambda(t) = \lambda(t) - \lambda_0$, with $\lambda_0 = 1541.37$ nm. The results are plotted in Fig. 5. We observe a maximum excursion of 12 pm (1.5 GHz) during the 12 days of acquisition. We found 8 pm at worst over one day, and typically a periodic oscillation of 3 pm (500 MHz) over two days. This measurement is also limited by the noise floor of our OSA, since we obtain a similar result when measuring one of the ultra-stable sources at hand in our laboratory. Thus, this measurement only sets an upper limit to the wavelength stability σ_λ over periods of days.

We denote similarly the resulting free running propagation delay fluctuations arising from wavelength fluctuations as Φ_λ. Similar to the temperature contribution, we can also compute the propagation delay fluctuation contribution Φ_λ in this worst case scenario, taking into account the chromatic dispersion coefficient of 17 ps/nm/km and the length of the link. We obtain a contribution to the propagation delay fluctuations $\Phi_\lambda = 6$ ps at 10^5 s.

D. Frequency Stability Analysis

We summarize the situation by plotting in Fig. 6(a) the OADEV for Φ_{WR}, Φ_T and Φ_λ. Temperature-induced propagation delay fluctuations are by far the dominant term. Chromatic dispersion contributes no more than 6×10^{-17} at one day of integration time for this first span of our cascaded link. This propagation delay contribution is even much smaller than the time delay fluctuations.

By extrapolation to one second integration time of the red line in Fig. 6, assuming that the nature of the laser noise remains white frequency noise, we can quantify the contribution from chromatic dispersion for a single-span of 125 km to the OADEV of the relative frequency fluctuations to be $< 5.4 \times 10^{-13}$ at one second. The corresponding linewidth at one second integration time of the 1541-nm long range SFP would be inferred as 0.18 pm (≈6 MHz). We deduced from these figures that chromatic dispersion should limit the short-term stability of WR links for long-haul links of length > 250 km, with such DWDM SFP emitters.

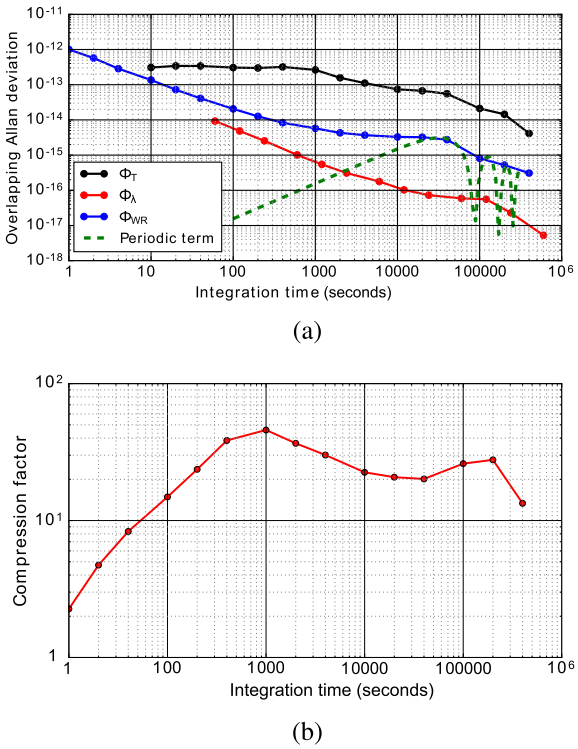

Fig. 6. Experimental results for the first 125-km span. (a) Φ_{WR} denotes the time delay fluctuations of the Slave #1, Φ_T the propagation delay fluctuations of the free running link due to temperature, and Φ_λ the propagation delay fluctuations due to wavelength fluctuations of the emitter, and their respective OADEVs $\sigma_{WR}, \sigma_T, \sigma_\lambda$. Green dashed line: one-day periodic temperature oscillation contribution model. (b) Compression factor as a function of integration time.

From the FFT analysis of ΔT_i, we found a typical daily perturbation with a period of 86 400 s and an amplitude of 1.6 K. Taking into account a factor readily given by $\Phi_T/\Phi_{WR} \simeq 20$ at 20 000–1 00 000-s measurement time we can compute the contribution of this periodic term to the OADEV, displayed as a green dashed line in Fig 6(a). We observe that the behavior of the OADEV after 40 000 s is still governed by the harmonics of daily fluctuations [59].

We define then a compression factor k_{dev} as the ratio between the OADEV of the relative frequency fluctuations corresponding to Φ_T and Φ_{WR}, as a function of the integration time τ, in Fig. 6(b). We observe that the compression factor reaches a maximum of 40 at τ =100 s. Then k_{dev} decreases down to 20–30 for longer integration times.

This limitation of the compression factor cannot be understood with a simple model of a WR link and the model presented for the action of temperature on the propagation delay, nor by the action of chromatic dispersion (see the details and underlying hypotheses in the Appendix). This is surprising as the noise floor of the WR switches or the counter are not yet reached and are well below the level of Φ_{WR} [32]. We checked that the delay fluctuations do not arise from the temperature sensitivity of the electronics or of the emitters. Indeed this behavior is not observed at the GM stage, which remains well below the 10^{-14} level [35]. This stability of the switches with temperature is consistent with other data reported in the literature [60] and more complete studies on the effect of temperature on a WR link [61]. We believe that

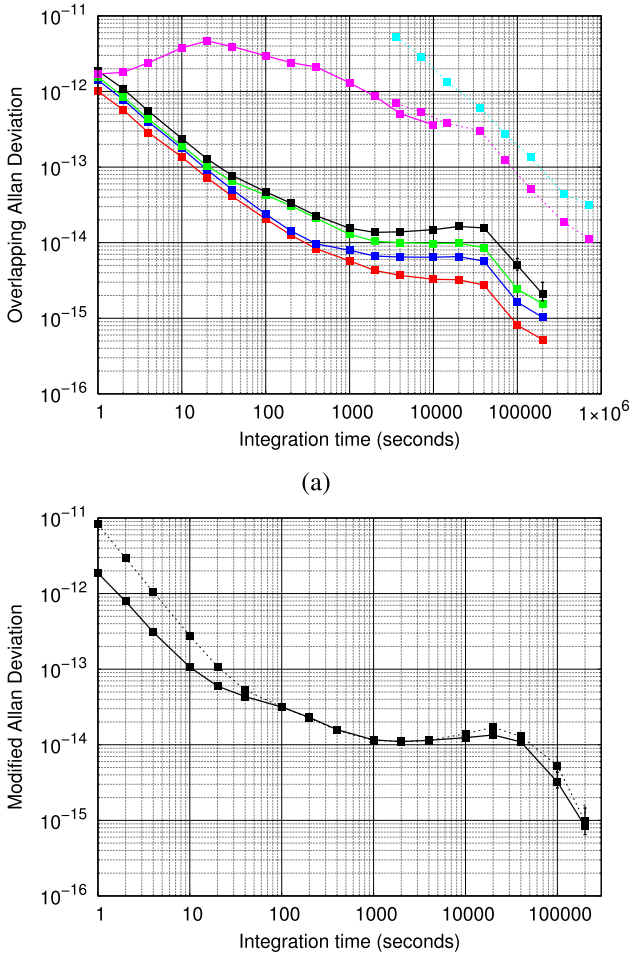

Fig. 7. (a) OADEV for the uni-directional 4-span cascaded White Rabbit link. f_{PTP} = 14 Hz, f_{BW} = 70 Hz. Span length = 125 km. Total length = 500 km. Red trace: 1 span, blue trace: 2 spans, green trace: 3 spans, black trace: 4 spans. GPS systems: Oscilloquartz 5201 (magenta trace), Quartzlock E8000 (cyan trace). Solid lines represent stability calculated from frequency data and dashed lines represent stability calculated from time data (PPS output). (b) Modified Allan Deviation for the output of the complete link, i.e., after the 4th span, for frequency data (black plain line) and time delay data (black dashed line).

this limitation could arise either from a wrong operation or bad parameter inputs of the link, either from an asymmetry of the link, originated from more fundamental physical reason related to the reciprocity of propagation of light in the two fibers.

E. Instability of a Cascaded Link

The OADEVs of the transferred frequencies for each of the cascaded spans are presented in Fig. 7(a) (see caption for details). The magenta and cyan traces are discussed in Section IV.

For the first span at 125 km, we obtain a frequency stability of 1×10^{-12} at one second of integration time. The stability scales down as τ^{-1} initially and then degrades, showing a maximum of 3×10^{-15} at $\tau \simeq 20\,000$ s. At 1 00 000 s of integration time, the frequency stability for this 125-km span reaches 8×10^{-16}.

For an N-span cascaded White-Rabbit link of identical span length L, one would expect the stability to scale by a factor

of $\sqrt{N}$. Indeed we observe that the stability after each span degrades as the length of the link increases, and we attain a value of 2×10^{-12} at $\tau = 1$ s for the 500-km link. The stability degrades for each consecutive span by a factor $\sqrt{N}$ at $\tau = 1$ s.

At long integration times, the stability degrades by a factor of approximately N for the first three spans, which is expected for our set-up where the thermal noise dominates at long times and is in common-mode for all the spans. For the last span, using the ZEN, we observe an excess of noise with a ratio $\sigma_y^{\text{span4}}/\sigma_y^{\text{span1}}$ greater than N by almost a factor of 1.5 at one day of integration time. In addition, we note that the ratio between the OADEVs for each span is not constant with varying integration time. It highlights that the cascaded approach provides an improvement depending on the nature of the dominant noise process at a given integration time, what we believe to be interesting is to compare to experimental observations with other optical links as, for instance, reported in [1], [62], and [63].

Fig. 7(b) presents the modified Allan deviation (MDEV) for the frequency and time (PPS) signals from the end-user ZEN equipment, i.e., after the complete 500-km link. As expected, the PPS output has the higher short-term noise, and there is good agreement between the two datasets in the long term [64]. This highlights the fact that improvement of the WR switch local oscillator phase noise only impacts the short-term stability of the frequency transfer.

F. Accuracy

We evaluate the accuracy of the frequency transfer of the cascaded WR-PTP link for each span, from the frequency data. We calculate the arithmetic mean of the difference between the expected and the measured frequency. The statistical uncertainty is estimated by the instability of the dataset at an appropriate averaging time [65], [66]. For the successive spans, we found, respectively, 29, 87, 404, and 16 165 outliers in a $\pm10^{-11}$ filter, which were removed from the dataset. The number of outliers is clearly higher for the last stage, as the Slave #4 went out of lock for four consecutive hours resulting in approximately 12 000 removed points. Still the Slave #4 keeps a good ratio of 99% of validated data points. The dataset is therefore almost phase continuous. The mean values of the relative frequency data and their associated statistical uncertainties, as quantified by the last value of the OADEV, for the successive spans are $(-1.1 \pm 60) \times 10^{-17}$, $(-4.0 \pm 100)\times10^{-17}$, $(-9.2 \pm 150)\times10^{-17}$, and $(-1.4 \pm 20)\times10^{-16}$, respectively. It is important to notice that the mean value for each of the spans is below the statistical uncertainty of the dataset. In conclusion, we do not observe any frequency shifts within the statistical uncertainty.

IV. Discussion

At short integration time, the limitations are mainly due to the electronic noise floor of the system [34]. For a sufficiently long link, the short-term stability performance may be limited by chromatic dispersion, due to the wavelength instability of the optical emitters (SFPs). Here, we found that in our experimental conditions, chromatic dispersion is expected to be dominant in the short term for links longer than 250 km. An established alternative is to use systems with embedded narrow-linewidth and temperature stabilized lasers [9]. However, for the use of active optical networks with a reduced cost of operation, working with standardized SFPs is an important advantage, as customized laboratory emitters are more difficult to implement. The cascaded approach used here seems to us to be a practical way to circumvent the effect of chromatic dispersion for the most demanding applications, which need good stability but don't require fully bidirectional operation as in [7]. This approach also fits well with the goal of multi-user time and frequency dissemination at a regional scale.

At mid- and long-term the OADEV lies well below 1×10^{-14} for the consecutive spans after 1 00 000-s integration time. The OADEV after 1000 s of integration time is governed by the fiber propagation noise. As shown in Fig. 6, the compression factor k_{dev} shows some limitations for integration time larger than 1000 s. It limits the performance of the WR-PTP link in our laboratory experiment. One would expect much higher compression factor values from a linear servo loop system. This could be due to some technical limitations, such as non-optimal parameterization of the SoftPLL and/or the WR engine, mistakes in the phase comparator (that is to say, the digital dual mixer time difference meter implemented in the FPGA at the heart of the WR engine [67]), or mistakes in the servo loop physical model. It could also be due to an asymmetry in the propagation delay for the forward and backward signal that was not well taken into account in our model, possibly linked to more fundamental reasons such as the effect of temperature on birefringence of the fiber as reported recently in the optical domain with fiber spools [68], [69].

For comparison, we present in Fig. 7, the frequency stability performance of two good quality commercial GPS receivers. Both receivers were measured at LNE-SYRTE, Paris, France, with respect to the 10-MHz signal derived from an active H-maser and/or with respect to UTC(OP). The Quartzlock E8000 does not filter the GPS signal with a good low noise oscillator, so the relative frequency stability at short integration times is poor and only time interval measurements were done between the PPS output and UTC(OP). The Oscilloquartz GPS receiver 5201 is equipped with a low-noise ultra-stable local oscillator (BVA 8601). We recorded the frequency deviation of the 10-MHz output versus a reference 10-MHz signal representing UTC(OP) and the time interval between the PPS output of the GPS receiver and UTC(OP). For the Oscilloquartz GPS receiver, we observe a short-term stability of 2×10^{-12} at one second of integration time, similar to the WR-PTP link. For longer integration time, at 1000 s, the cascaded WR-PTP link has a better performance by at least one order of magnitude when compared to both the GPS receivers. We also note that the cascaded 500-km WR-PTP link attains a frequency stability of 1×10^{-13} at an integration time of less than 40 s, whereas the GPS systems attain the same level of performance after more than 80 000 s of integration time.

V. Conclusion

We demonstrate for the first time the effect of a high PTP rate on the clock output of a WR-PTP link. We combine

this with a three-times higher than usual SoftPLL bandwidth for locking the local oscillator of White Rabbit switches. We demonstrate high-performance frequency dissemination using White Rabbit PTP for a cascaded long-haul link of 500 km. We achieve a short-term frequency stability of 1×10^{-12} for the 125-km span, while due to the cascaded approach, the short-term frequency stability for a 500-km link is 2×10^{-12}. With the cascaded approach, where the uni-directional link length L is divided into N segments of equal lengths, the chromatic dispersion contribution scales as $L/\sqrt{N}$ instead of L. Thus with $N = 4$, we improve the short-term stability of the complete link by a factor of 2.

We show here excellent performance for a WR link using a cascade approach. The modifications consisted in adding a single capacitor to the hardware of the GrandMaster, and in firmware modifications. In the long term, at 1 00 000 s, the frequency stability achieved for a 125-km span is approximately 1×10^{-15}, and 5×10^{-15} for the full 500-km link. No frequency shift was observed within the statistical uncertainty of the dataset.

We observed key properties of the cascaded link, scaling as the square root of the number of hops at short times, and with a linear scaling with the number of hops at long times. This sheds an interesting light on the nature of noise in such links and shows that the improvement given by the cascaded approach depends on the dominant noise properties. Furthermore, we showed that the compression factor of our WR link is below expectations, which indicates a possible major source of improvement for WR links.

However, the long-term stabilities shown in this report are already quite low, at the 10^{-15} level, which already meets the long-term stability of many primary frequency standards. Thus, such a level of performance should satisfy most potential end-users.

With such levels of performance, White Rabbit PTP is expected to enable frequency dissemination at a regional or national scale with a long-term frequency stability one order of magnitude better than GNSS-based methods. More importantly in our opinion, remote calibration at the 10^{-14} level within one hour of measurement time could be achieved at industry facilities. Such levels of performance meet the requirements of many industrial and civil applications. It also opens very interesting possibilities for the generation of national atomic time scales and the frequency disciplining of industrial clocks (Cs, Rb, H-maser). These links appear as a good candidate to bridge the gap between performance, competitive cost, and scalability.

Appendix
Compensation for Thermal Fiber Noise and Chromatic Dispersion

In this appendix, we present a compensation model for WR-PTP links, and focus our attention on the instability contributions arising from temperature fluctuations, acting on the optical length of the link, and from fluctuations of the emitted wavelengths, perturbing the delay measurement through chromatic dispersion, for the case of a uni-directional link.

A. Compensation Model

PTP uses a simple two-way time transfer to measure the time offset between a Master clock and a Slave clock, and PTP implementations use this measurement to synchronize the Slave clock. Let D_{MS} be the signal propagation duration from Master to Slave, and D_{SM} the propagation duration from Slave to Master. Any uncorrected difference between D_{MS} and D_{SM}, also referred to as an asymmetry, will cause a phase offset of the Slave clock, θ_{WR}, given in the simplest analysis and up to a sign by

$$\theta_{\mathrm{WR}} = \frac{D_{\mathrm{MS}} - D_{\mathrm{SM}}}{2}. \tag{1}$$

We note that PTP in general, and WR-PTP in particular, includes calibration methods which correct for many sources of such link asymmetries. The numerator of this equation should be understood to include only contributions to the difference between D_{MS} and D_{SM} for which no such correction is made.

It follows that fluctuations δD_{MS} and δD_{SM} of the two propagation delays cause fluctuations Φ_{WR} of the Slave clock phase given by:

$$\Phi_{\mathrm{WR}} = \frac{\delta D_{\mathrm{MS}} - \delta D_{\mathrm{SM}}}{2} \tag{2}$$

where again the numerator should be understood to include only contributions for which no correction is made.

B. Effect of Temperature Fluctuations for a Uni-Directional Link

We assume a uniform temperature over the whole length of fiber, equal for the two fibers, and varying with time. For a temperature change δT, the variation of the propagation delays due to the changes in optical length of the two fibers can be written as

$$\begin{cases} \delta D_{\mathrm{MS}} = \kappa L_{\mathrm{MS}} \delta T \\ \delta D_{\mathrm{SM}} = \kappa L_{\mathrm{SM}} \delta T \end{cases} \tag{3}$$

where L_{MS} and L_{SM} are the lengths of the two fibers and κ is a proportionality coefficient, assumed to be positive and equal for the two fibers. For integration times long enough compared to the propagation time and the thermalization time of the fibers, the temperature changes for the photon's trip forth and back are fully correlated, so one can write the resulting Slave clock phase fluctuations as

$$\Phi_{\mathrm{WR,T}} = \frac{\kappa(L_{\mathrm{MS}} - L_{\mathrm{SM}})}{2}\delta T. \tag{4}$$

This is the closed loop time delay fluctuation. The contribution to the Allan deviation of Φ_{WR} from this effect is

$$\sigma_{\mathrm{WR,T}} = \frac{\kappa|L_{\mathrm{MS}} - L_{\mathrm{SM}}|}{2}\sigma_{\mathrm{T}} \tag{5}$$

where σ_{T} is the Allan deviation of δT.

In comparison, the open loop propagation delay fluctuation, as used in Section III-B, is

$$\Phi_{\mathrm{T}} = \delta D_{\mathrm{MS}} = \kappa L_{\mathrm{MS}} \delta T \tag{6}$$

and its Allan deviation is

$$\sigma_T = \kappa L_{MS} \sigma_T. \tag{7}$$

Defining the compression factor k_{dev} to be the ratio between σ_T and $\sigma_{WR,T}$, analogously to Section III-D, we obtain

$$k_{dev} = \frac{2L_{MS}}{|L_{MS} - L_{SM}|}. \tag{8}$$

In the case presented in this article, fiber thermal noise dominates the relative frequency stability at integration times greater than 1000 s. We measured the asymmetry of the link by measuring the time offset at the Slave stages with respect to the GM with a cascaded short fiber link cable and with the 125-km spools arrangement. The asymmetry of our link is difficult to measure and we did not do this very accurately. However, optical time delayed reflectometry measurement confirmed the length asymmetry to be of the order of 100 m. Thus the asymmetry $|L_{MS} - L_{SM}|/L_{MS}$ of our fiber spools arrangement is about $8 \pm 1 \times 10^{-4}$, which gives $k_{dev} \simeq 2500$. If one compares these figures with the plot reported in Fig. 6(b), one observes that the actual limitations of the compression factor cannot be explained by the influence of temperature fluctuations on the propagation delay asymmetry.

It can be noticed that in the case of a WR link with a 1310-nm/1490-nm emitter pair over a single fiber, an analogous asymmetry arises from the refractive index difference of about 2.6×10^{-4}. The noise limitation will then depend on the length of the link.

C. Effect of Wavelength Fluctuations for a Uni-Directional Link

WR uses amplitude modulated laser diodes for data transmission. The wavelength of emission λ is not perfectly stable over the time, and chromatic dispersion leads to a time dependent propagation delay fluctuation. One can write the delay fluctuations for the Master $\rightarrow$ Slave δD_{MS} and Slave $\rightarrow$ Master δD_{SM} as

$$\begin{cases} \delta D_{MS} = \kappa' L_{MS} \delta\lambda_1 \\ \delta D_{SM} = \kappa' L_{SM} \delta\lambda_2 \end{cases} \tag{9}$$

where $\delta\lambda_1$ and $\delta\lambda_2$ are the wavelength fluctuations in the two directions, and κ' is a proportionality coefficient, assumed to be equal for the two directions of propagation. Using (2), the Slave clock phase fluctuations (closed loop time delay fluctuations) due to the laser instability are

$$\Phi_{WR,\lambda} = \frac{\kappa'}{2}(L_{MS}\delta\lambda_1 - L_{SM}\delta\lambda_2). \tag{10}$$

Assuming that $\delta\lambda_1$ and $\delta\lambda_2$ are independent random variables having the same Allan deviation σ_λ, the Allan deviation of the closed loop fluctuations of the Slave clock phase due to wavelength instability is

$$\sigma_{WR,\lambda} = \frac{|\kappa'|}{2}\sqrt{L_{MS}^2 + L_{SM}^2}\,\sigma_\lambda \simeq \frac{|\kappa'|L_{MS}}{\sqrt{2}}\sigma_\lambda \tag{11}$$

where we also assume that $L_{MS} \simeq L_{SM}$. We repeat that this formula arises from the hypothesis that the wavelength noises of the two emitters are uncorrelated.

In open loop, the propagation delay fluctuations are

$$\Phi_\lambda = \delta D_{MS} = \kappa' L_{MS} \delta\lambda_1. \tag{12}$$

Defining the compression factor as $k_{dev} = \sigma_\lambda/\sigma_{WR,\lambda}$ at any time that satisfies the hypotheses of time intervals larger than the round-trip time and of uncorrelated noise, and noting that the only time-dependent variable is the wavelength fluctuation, one finds that $k_{dev} \simeq \sqrt{2}$.

For integration times long enough compared to the propagation time, and for in-field applications, the wavelength changes at the two ends of the link are probably uncorrelated. At long integration times, when the thermal fiber noise is sufficiently suppressed, chromatic dispersion sets therefore an ultimate limit for the performances of WR links using standard 1G telecom SFPs.

In the case of our in-lab experiment, one can expect a partial correlation of the wavelength fluctuations in the long term, and partial suppression of the delay fluctuations induced by the wavelength instability of the emitters. This does not affect the results we present here, as the chromatic dispersion contribution to the total instability at long integration times is much less than the contribution from the thermal fiber noise, as shown in Fig. 6.

ACKNOWLEDGMENT

The authors would like to thank Javier Díaz, Rafa Rodriguez, and J. Gabriel Ramírez at Seven Solutions, Spain, and Felipe Torres Gonzalez at the University of Granada, Spain, for their collaboration and help. They would also like to thank people involved in the WR project for their continuous stimulation and sharing issues through the mailing list, and to thank especially Javier Serrano, Alessandro Rubini, T. Wlostowski, and Mattia Rizzi at CERN, Switzerland and France, for their help and support. They would also like to thank Michel Abgrall and Baptiste Chupin for their support in using the UTC(OP) signals and for measurements in their laboratory. They would also like to thank Michel Lours for technical support and his advices. They would also like to thank Gesine Grosche and Sebastian Koke for providing a Quartzlock E8000 for testing at LNE-SYRTE, Paris, France. They would also like to thank David Valat from CNES for providing the Physipus STS201 for their experiment.

REFERENCES

[1] N. Chiodo *et al.*, "Cascaded optical fiber link using the internet network for remote clocks comparison," *Opt. Exp.*, vol. 23, no. 26, pp. 33927–33937, Dec. 2015.

[2] S. M. F. Raupach, A. Koczwara, and G. Grosche, "Brillouin amplification supports 1×10^{-20} uncertainty in optical frequency transfer over 1400 km of underground fiber," *Phys. Rev. A, Gen. Phys.*, vol. 92, no. 2, Aug. 2015, Art. no. 021801, doi: 10.1103/PhysRevA.92.021801.

[3] C. Lisdat *et al.*, "A clock network for geodesy and fundamental science," *Nature Commun.*, vol. 7, p. 12443, Aug. 2016. [Online]. Available: https://www.nature.com/articles/ncomms12443

[4] J. Guéna *et al.*, "First international comparison of fountain primary frequency standards via a long distance optical fiber link," *Metrologia*, vol. 54, no. 3, p. 348, 2017. [Online]. Available: http://stacks.iop.org/0026-1394/54/i=3/a=348

[5] P. Delva *et al.*, "Test of special relativity using a fiber network of optical clocks," *Phys. Rev. Lett.*, vol. 118, no. 22, Jun. 2017, Art. no. 221102, doi: 10.1103/PhysRevLett.118.221102.

[6] J. Grotti *et al.*, "Geodesy and metrology with a transportable optical clock," *Nature Phys.*, vol. 14, no. 5, p. 437, 2018. [Online]. Available: https://www.nature.com/articles/s41567-017-0042-3

[7] P. Krehlik, L. Sliwczynski, L. Buczek, J. Kolodziej, and M. Lipinski, "ELSTAB—Fiber-optic time and frequency distribution technology: A general characterization and fundamental limits," *IEEE Trans. Ultrason., Ferroelectr., Freq. Control*, vol. 63, no. 7, pp. 993–1004, Jul. 2016.

[8] Ł. Śliwczyński, P. Krehlik, Ł. Buczek, and M. Lipiński, "Active propagation delay stabilization for fiber-optic frequency distribution using controlled electronic delay lines," *IEEE Trans. Instrum. Meas.*, vol. 60, no. 4, pp. 1480–1488, Apr. 2011.

[9] P. Krehlik, Ł. Sliwczynski, Ł. Buczek, and M. Lipinski, "Fiber-optic joint time and frequency transfer with active stabilization of the propagation delay," *IEEE Trans. Instrum. Meas.*, vol. 61, no. 10, pp. 2844–2851, Oct. 2012.

[10] L. Sliwczynski and P. Krehlik, "Multipoint joint time and frequency dissemination in delay-stabilized fiber optic links," *IEEE Trans. Ultrason., Ferroelectr., Freq. Control*, vol. 62, no. 3, pp. 412–420, Mar. 2015. [Online]. Available: http://ieeexplore.ieee.org/document/7055436/

[11] O. Lopeza *et al.*, "Frequency and time transfer for metrology and beyond using telecommunication network fibres," *Comp. Rendus Phys.*, vol. 16, no. 5, pp. 531–539, Jun. 2015. [Online]. Available: https://hal.archives-ouvertes.fr/hal-01176012

[12] D. R. Gozzard, S. W. Schediwy, and K. Grainge, "Simultaneous transfer of stabilized optical and microwave frequencies over fiber," *IEEE Photon. Technol. Lett.*, vol. 30, no. 1, pp. 87–90, Jan. 1, 2018. [Online]. Available: http://ieeexplore.ieee.org/document/8116672/

[13] D. P. Venmani, O. L. Moult, F. Deletre, Y. Lagadec, and Y. Morlon, "On the role of network synchronization for future cellular networks: An operator's perspective," *IEEE Commun. Mag.*, vol. 54, no. 9, pp. 58–64, Sep. 2016.

[14] R. Razzaghi, A. Derviskadic, and M. Paolone, "A White Rabbit synchronized PMU," in *Proc. IEEE PES Innov. Smart Grid Technol. Conf. Eur. (ISGT-Europe)*, Sep. 2017, pp. 1–6.

[15] J. Allnutt *et al.* (2017). *Timing Challenges in the Smart Grid*. [Online]. Available: http://nvlpubs.nist.gov/nistpubs/SpecialPublications/NIST.SP.1500-08.pdf

[16] M. A. Lombardi, A. N. Novick, G. Neville-Neil, and B. Cooke, "Accurate, traceable, and verifiable time synchronization for world financial markets," *J. Res. Nat. Inst. Standards Technol.*, vol. 121, p. 436, Oct. 2016. [Online]. Available: https://nvlpubs.nist.gov/nistpubs/jres/121/jres.121.023.pdf

[17] K. G. Baldwin *et al.*, "Dissemination of precise radio-frequency references for environmental sensing over long-haul optical-fiber networks," in *Proc. Conf. Opt. Photon. Energy Environ.*, 2016, Paper ETu3A.3. [Online]. Available: https://www.osapublishing.org/abstract.cfm?URI=EE-2016-ETu3A.3, doi: 10.1364/EE.2016.ETu3A.3.

[18] G. Marra *et al.*, "Ultrastable laser interferometry for earthquake detection with terrestrial and submarine cables," *Science*, vol. 361, no. 6401, pp. 486–490, Aug. 2018. [Online]. Available: http://science.sciencemag.org/content/early/2018/06/13/science.aat4458

[19] Ł. Śliwczyński, P. Krehlik, and M. Lipiński, "Optical fibers in time and frequency transfer," *Meas. Sci. Technol.*, vol. 21, no. 7, Jul. 2010, Art. no. 075302. [Online]. Available: http://stacks.iop.org/0957-0233/21/i=7/a=075302?key=crossref.5090936e280242cad1473de767396c14

[20] A. Bercy, F. Stefani, O. Lopez, C. Chardonnet, P.-E. Pottie, and A. Amy-Klein, "Two-way optical frequency comparisons at 5×10^{-21} relative stability over 100-km telecommunication network fibers," *Phys. Rev. A, Gen. Phys.*, vol. 90, no. 6, Dec. 2014, doi: 10.1103/PhysRevA.90.061802.

[21] K. Turza, A. Binczewski, W. Bogacki, P. Krehlik, and L. Sliwczynski, "Time and frequency transfer in modern DWDM telecommunication networks," in *Proc. Joint Conf. Eur. Freq. Time Forum IEEE Int. Freq. Control Symp. (EFTF/IFC)*, Jul. 2017, pp. 368–370. [Online]. Available: http://ieeexplore.ieee.org/document/8088894/

[22] L. Yu *et al.*, "WDM-based radio frequency dissemination in a tree-topology fiber optic network," *Opt. Exp.*, vol. 23, no. 15, p. 19783, 2015. [Online]. Available: https://www.osapublishing.org/abstract.cfm?URI=oe-23-15-19783

[23] K. Turza, P. Krehlik, and Ł. Śliwczyński, "Stability limitations of optical frequency transfer in telecommunication DWDM networks," *IEEE Trans. Ultrason., Ferroelectr., Freq. Control*, vol. 67, no. 5, pp. 1066–1073, May 2019.

[24] J. Serrano *et al.*, "The White Rabbit project," in *Proc. IBIC*, 2013, pp. 93–95. [Online]. Available: https://www.ohwr.org/attachments/2528/IBIC2013_WR.pdf

[25] M. Lipinski, T. Wlostowski, J. Serrano, and P. Alvarez, "White Rabbit: A PTP application for robust sub-nanosecond synchronization," in *Proc. IEEE Int. Symp. Precis. Clock Synchronization Meas., Control Commun. (ISPCS)*, Sep. 2011, pp. 25–30.

[26] O. Ronen and M. Lipinski, "Enhanced synchronization accuracy in IEEE1588," in *Proc. IEEE Int. Symp. Precis. Clock Synchronization Meas., Control, Commun. (ISPCS)*, Oct. 2015, pp. 76–81.

[27] J. L. Gutierrez-Rivas, C. Prados, and J. Diaz, "Sub-nanosecond synchronization accuracy for time-sensitive applications on industrial networks," in *Proc. Eur. Freq. Time Forum (EFTF)*, Apr. 2016, pp. 1–4. [Online]. Available: http://ieeexplore.ieee.org/document/7477794/

[28] J. L. Gutierrez-Rivas, J. Lopez-Jimenez, E. Ros, and J. Diaz, "White Rabbit HSR: A seamless subnanosecond redundant timing system with low-latency data capabilities for the smart grid," *IEEE Trans. Ind. Informat.*, vol. 14, no. 8, pp. 3486–3494, Aug. 2018.

[29] *IEEE Standard for a Precision Clock Synchronization Protocol for Networked Measurement and Control Systems*, IEEE Standard 1588-2019 (Revision of IEEE Std 1588-2008), 2020, pp. 1–499.

[30] E. F. Dierikx *et al.*, "White Rabbit precision time protocol on long-distance fiber links," *IEEE Trans. Ultrason., Ferroelectr., Freq. Control*, vol. 63, no. 7, pp. 945–952, Jul. 2016. [Online]. Available: http://ieeexplore.ieee.org/document/7383303/

[31] A. Wallin, M. Rizzi, G. M. Calvés, T. Fordell, and J. Näränen, "Improved systematic and random errors for long-distance time-transfer using PTP White Rabbit," in *Proc. 32nd Eur. Freq. Time Forum (EFTF)*, 2018. [Online]. Available: https://cris.vtt.fi/en/publications/improved-systematic-and-random-errors-for-long-distance-time-tran

[32] M. Rizzi. (2016). *OHR White Rabbit Low Jitter*. [Online]. Available: https://www.ohwr.org/projects/wr-low-jitter/documents

[33] C. Tour and J. C. J. Koelemeij. (2017). *Sub-Nanosecond Time Accuracy and Frequency Distribution Through White Rabbit Ethernet*. [Online]. Available: https://library.nrao.edu/public/memos/ngvla/NGVLA_22.pdf

[34] M. Rizzi, M. Lipinski, P. Ferrari, S. Rinaldi, and A. Flammini, "White Rabbit clock synchronization: Ultimate limits on close-in phase noise and short-term stability due to FPGA implementation," *IEEE Trans. Ultrason., Ferroelectr., Freq. Control*, vol. 65, no. 9, pp. 1726–1737, Sep. 2018. [Online]. Available: https://ieeexplore.ieee.org/document/8400550/

[35] N. Kaur, P. Tuckey, and P. E. Pottie, "Time transfer over a White Rabbit network," in *Proc. Eur. Freq. Time Forum (EFTF)*, Apr. 2016, pp. 1–4.

[36] F. Girela-Lopez, F. Torres-Gonzalez, and J. Diaz, "Ultra-accurate Ethernet time-transfer with programmable carrier-frequency based on White Rabbit solution," in *Proc. IEEE Int. Symp. Precis. Clock Synchronization Meas., Control, Commun. (ISPCS)*, Aug. 2017, pp. 1–6.

[37] H. Z. Peek, T. J. Pinkert, P. P. M. Jansweijer, and J. C. J. Koelemeij, "Measurement of optical to electrical and electrical to optical delays with ps-level uncertainty," *Opt. Exp.*, vol. 26, no. 11, pp. 14650–14660, 2018. [Online]. Available: https://www.osapublishing.org/oe/abstract.cfm?uri=oe-26-11-14650

[38] A. Wujek, G. Daniluk, M. Lipinski, and A. Rubini, "Managing your timing system as a standard Ethernet network," in *Proc. 16th Int. Conf. Accel. Large Exp. Control Syst. (ICALEPCS)*, 2017, pp. 1–5. [Online]. Available: http://jacow.org/icalepcs2017/doi/JACoW-ICALEPCS2017-TUSH303.html

[39] M. Jimenez-Lopez, F. Torres-Gonzalez, J. L. Gutierrez-Rivas, M. Rodriguez-Alvarez, and J. Diaz, "A fully programmable White-Rabbit node for the SKA telescope PPS distribution system," *IEEE Trans. Instrum. Meas.*, vol. 68, no. 2, pp. 632–641, Feb. 2019. [Online]. Available: https://ieeexplore.ieee.org/document/8412745/

[40] T. Fordell and A. Wallin, "A simple high-performance remote-maser concept," in *Proc. 32nd Eur. Freq. Time Forum (EFTF), Abstr.*, 2018, p. 143. [Online]. Available: https://cris.vtt.fi/en/publications/a-simple-high-performance-remote-maser-concept

[41] J. Serrano. (2017). *OHR WR Users*. [Online]. Available: https://www.ohwr.org/projects/white-rabbit/wiki/WRUsers

[42] M. Jimenez-Lopez, J. L. Gutierrez-Rivas, J. Diaz, E. Lopez-Marin, and R. Rodriguez, "WR-ZEN: Ultra-accurate synchronization SoC based on Zynq technology," in *Proc. Eur. Freq. Time Forum (EFTF)*, Apr. 2016, pp. 1–4.

[43] C. Champion, M. Punch, R. Oger, S. Colonges, and Y. Moudden, "TiCkS: A flexible White-Rabbit based time-stamping board," 2017, *arXiv:1710.07128*.

[44] O. Lopez *et al.*, "Cascaded multiplexed optical link on a telecommunication network for frequency dissemination," *Opt. Exp.*, vol. 18, no. 16, pp. 16849–16857, Aug. 2010. [Online]. Available: https://www.osapublishing.org/abstract.cfm?uri=oe-18-16-16849

[45] F. Torres-Gonzalez, J. Diaz, E. Marin-Lopez, and R. Rodriguez-Gomez, "Scalability analysis of the White-Rabbit technology for cascade-chain networks," in *Proc. IEEE Int. Symp. Precis. Clock Synchronization Meas., Control, Commun. (ISPCS)*, Sep. 2016, pp. 1–6. [Online]. Available: http://ieeexplore.ieee.org/document/7579515/

[46] G. D. Rovera *et al.*, "UTC(OP) based on LNE-SYRTE atomic fountain primary frequency standards," *Metrologia*, vol. 53, no. 3, pp. S81–S88, Jun. 2016. [Online]. Available: http://stacks.iop.org/0026-1394/53/i=3/a=S81?key=crossref.53341e3aeae3b01541e619ae253578d9

[47] M. Rizzi, "White Rabbit switch performance in grandmaster mode," CERN, Switzerland, Tech. Rep., 2016, p. 20. [Online]. Available: https://www.ohwr.org/documents/475, doi: 10.1109/ISPCS.2016.7579514.

[48] N. Kaur, F. Frank, P.-E. Pottie, and P. Tuckey, "Time and frequency transfer over a 500 km cascaded White Rabbit network," in *Proc. Joint Conf. Eur. Freq. Time Forum IEEE Int. Freq. Control Symp. (EFTF/IFCS)*, Jul. 2017, pp. 86–90.

[49] N. Kaur, "Long range time transfer with optical fiber links and cross comparisons with satellite based methods," Ph.D. dissertation, Dept. SYRTE, PSL Univ. Paris, Paris, France, 2018. [Online]. Available: https://tel.archives-ouvertes.fr/tel-02089265

[50] J. Díaz. (2017). *Switch_ohr*. [Online]. Available: https://www.ohwr.org/projects/white-rabbit/wiki/switch

[51] E. Samain, P. Fridelance, and P. Guillemot, "An ultra stable event timer designed for T2L2," in *Proc. 24th EFTF*, 2010, pp. 142–147. [Online]. Available: https://www.eftf.org/proceedings/

[52] P. Exertier *et al.*, "T2L2: Five years in space," in *Proc. Joint Eur. Freq. Time Forum Int. Freq. Control Symp. (EFTF/IFC)*, Jul. 2013, pp. 632–635.

[53] *Faq Switch Wiki Projects/White Rabbit*. Accessed: Nov. 5, 2021. [Online]. Available: https://ohwr.org/project/white-rabbit/wikis/FAQswitch

[54] M. Rizzi *et al.*, "White Rabbit clock characteristics," in *Proc. IEEE Int. Symp. Precis. Clock Synchronization Meas., Control, Commun. (ISPCS)*, Sep. 2016, pp. 1–6. [Online]. Available: http://ieeexplore.ieee.org/document/7579514/

[55] M. J. López, *Distributed Control Systems Based on High Accurate Timing Synchronization*. Granada, Spain: Universidad de Granada, 2019. [Online]. Available: https://digibug.ugr.es/handle/10481/54816

[56] W. J. Riley, *Handbook of Frequency Stability Analysis*, vol. 31, no. 1. Washington, DC, USA: U.S. Department of Commerce, National Institute of Standards and Technology, 1994.

[57] L. G. Cohen and J. W. Fleming, "Effect of temperature on transmission in lightguides," *Bell Syst. Tech. J.*, vol. 58, no. 4, pp. 945–951, 1979.

[58] F. Stefani *et al.*, "Tackling the limits of optical fiber links," *J. Opt. Soc. Amer. B, Opt. Phys.*, vol. 32, no. 5, pp. 1–12, 2014.

[59] D. A. Howe, "Interpreting oscillatory frequency stability plots," in *Proc. IEEE Int. Freq. Control Symp. PDA Exhibit.*, May 2002, pp. 725–732.

[60] P. P. M. Jansweijer, H. Z. Peek, and E. de Wolf, "White Rabbit: Sub-nanosecond timing over ethernet," *Nucl. Instrum. Methods Phys. Res. A, Accel. Spectrom. Detect. Assoc. Equip.*, vol. 725, pp. 187–190, Oct. 2013. [Online]. Available: http://linkinghub.elsevier.com/retrieve/pii/S016890021201652X

[61] H. Li, G. Gong, W. Pan, Q. Du, and J. Li, "Temperature effect on White Rabbit timing link," *IEEE Trans. Nucl. Sci.*, vol. 62, no. 3, pp. 1021–1026, Jun. 2015. [Online]. Available: http://ieeexplore.ieee.org/document/7117457/

[62] M. Fujieda, M. Kumagai, and S. Nagano, "Coherent microwave transfer over a 204-km telecom fiber link by a cascaded system," *IEEE Trans. Ultrason., Ferroelectr., Freq. Control*, vol. 57, no. 1, pp. 168–174, Jan. 2010.

[63] S. Koke *et al.*, "Combining fiber Brillouin amplification with a repeater laser station for fiber-based optical frequency dissemination over 1400 km," *New J. Phys.*, vol. 21, no. 12, Dec. 2019, Art. no. 123017, doi: 10.1088/1367-2630/ab5d95.

[64] F. Frank, F. Stefani, P. Tuckey, and P.-E. Pottie, "A sub-ps stability time transfer method based on optical modems," *IEEE Trans. Ultrason., Ferroelectr., Freq. Control*, vol. 65, no. 6, pp. 1001–1006, Jun. 2018. [Online]. Available: https://ieeexplore.ieee.org/document/8354832/

[65] W.-K. Lee, D.-H. Yu, C. Y. Park, and J. Mun, "The uncertainty associated with the weighted mean frequency of a phase-stabilized signal with white phase noise," *Metrologia*, vol. 47, no. 1, p. 24, 2010. [Online]. Available: http://stacks.iop.org/0026-1394/47/i=1/a=004

[66] E. Benkler, C. Lisdat, and U. Sterr, "On the relation between uncertainties of weighted frequency averages and the various types of Allan deviations," *Metrologia*, vol. 52, no. 4, p. 565, 2015. [Online]. Available: http://stacks.iop.org/0026-1394/52/i=4/a=565

[67] P. Moreira, P. Alvarez, J. Serrano, I. Darwezeh, and T. Wlostowski, "Digital dual mixer time difference for sub-nanosecond time synchronization in Ethernet," in *Proc. IEEE Int. Freq. Control Symp.*, Jun. 2010, pp. 449–453. [Online]. Available: http://ieeexplore.ieee.org/document/5556289/

[68] D. Xu, O. Lopez, A. Amy-Klein, and P.-E. Pottie, "Polarization scramblers to solve practical limitations of frequency transfer," *J. Lightw. Technol.*, vol. 39, no. 10, pp. 3106–3111, May 15, 2021.

[69] D. Xu, O. Lopez, A. Amy-Klein, and P.-E. Pottie, "Nonreciprocity in optical fiber links: Experimental evidence," *Opt. Exp.*, vol. 29, no. 11, p. 17476, 2021. [Online]. Available: https://www.osapublishing.org/oe/abstract.cfm?doi=10.1364/OE.420661

Namneet Kaur received the B.Sc. and M.Sc. degrees in physics and electronics from Panjab University, Chandigarh, India, in 2011 and 2013, respectively, and the Ph.D. degree in long-range time transfer over optical fiber links from LNE-SYRTE, Paris, France, in 2018.

She is currently working on developing a traceable time as a service for critical infrastructures. Her research interests include high-performance time and frequency dissemination over optical fiber links, optical clock comparison, and its intriguing applications.

Florian Frank received the master's degree in electronics from ENSEIRB (the University of Bordeaux), Bordeaux, France, in 2007, and the Ph.D. degree in optoelectronics from Université Paris-Est, Paris, France, in 2011, conducted on radio over fiber in access networks at Orange Labs, Lannion, France.

From 2011 to 2015, he was with Ekinops, Lannion, as an Electronics Engineer. From 2016 to 2020, he was successively with the Syrte, Observatoire de Paris, Paris, and the Laboratoire de Physique des Lasers (LPL), Villetaneuse, France, as a Research Engineer working on time transfer over optical links. He is currently with Orange Labs, focusing on optical network architectures with an interest in non-linear impairments in coherent transmissions.

Jose Pinto, photograph and biography not available at the time of publication.

Philip Tuckey received the Ph.D. degree from Cambridge University, Cambridge, U.K., in 1988.

He is currently a Former Director of the SYRTE Department, Paris Observatory, Paris, France, and a Former Science Advisor to the Director General of French metrology. He coordinated the CLONETS Project on fiber links for time and frequency transfer in Europe.

Paul-Eric Pottie received the Ph.D. degree in physics from the University Pierre et Marie Curie, Paris, in 2003.

Since 2012, he has been working with LNE-SYRTE, Paris, France, on optical fiber links, for ultra-precise time and frequency transfer over long haul links and fiber networks. His research interests include time and frequency metrology, lasers, cold atoms frequency standards, and Bose-Einstein condensates.